Gas Breakdown in Microgaps With a Surface Protrusion on the Electrode

Yangyang Fu, *Member, IEEE*, Janez Krek, *Student Member, IEEE*, Peng Zhang, *Senior Member, IEEE*, and John P. Verboncoeur, *Fellow, IEEE*

***Abstract*— This paper summarizes our recent studies on a gas breakdown in microgaps with a surface protrusion on the electrode with more detailed information. The breakdown voltages are quantified when the discharge enters into the subnormal glow region with negative differential resistance, using a 2-D fluid model. The breakdown characteristics are evaluated with the effects of the protrusion geometries, such as protrusion size and aspect ratio, as well as the discharge polarity. It is found that in an atmospheric-pressure microgap, the protrusion size has a more profound effect on the breakdown voltage than its aspect ratio, which is due to the competition between the current density enhancement and the effective cathode emission area. As gas pressure varies, the surface protrusion on the electrode results in a combined Paschen's curve, which transits from long-gap behavior at low pressure to short-gap behavior at high pressure. The key parameters on the breakdown characteristics with the surface protrusion are elucidated.**

***Index Terms*— Discharge polarity, gas breakdown, microdischarge, Paschen's curve, surface protrusion, Townsend discharge.**

I. Introduction

MICRODISCHARGES with characteristic lengths of less than 1 mm become more attractive in recent years due to their numerous application potentials, including ion sources, microchip devices, and microswitches [1]–[5]. As is well known, Paschen's law was derived to describe the breakdown voltage as a function of a combined parameter pd (gas pressure $p \times$ gap distance d) in macrogaps under uniform electric field, which is an effective way to analyze the electrical properties and help to design device parameters for gas-insulated circuit breakers [6]–[11]. Similarly, the breakdown characteristics in microgaps have received growing interests as they are fundamental in understanding microdischarges in focused regimes. Nowadays, with the rise of 3-D printing capabilities, fabrication technologies enable manufacturing of increasingly complicated geometries, rather than planar ones, in plasma devices down to microscales [12], [13]. Previous studies indicate that the surface structure of the microgap, especially with the presence of the surface protrusion or surface roughness, could have a significant impact on the breakdown characteristics [14]–[16] and plasma sheath properties [17]. On the other hand, finishing the electrode surfaces would maximize voltage hold off. However, controlling the surface finish of the microgap electrode is difficult in microsystems. Even if the finish can be achieved during fabrication, surface roughening may still be introduced from "scratch and dig" during handling and assembly or from sputtering, microarcs, and deposition, where surface features are created. Under these situations, gas breakdown characteristics will be more complex and the effect of the microstructure on the electrode surface should be investigated.

Recently, Meng *et al.* [18], [19] conducted *in situ* optical observation of dynamic breakdown across microgaps (from 1 to 20 μm) and showed the transition between gas breakdown mechanisms and the morphology of the discharge path. As for the microdischarge breakdowns, taking the dc discharge, for example, recent studies indicate that it can be ignited with different cathode emission mechanisms, such as ion-impact secondary electron emission or field emission. Previous studies distinguished that the discharge is maintained by secondary electron emission when the gap distance is less than $\sim$10 μm, while the dominant process becomes electron field emission when the gap is less than a few micrometers [20]–[22]. More exactly, the field emission comes into play when the local electric field near the cathode is on the order of 10^9 V/m [2], [23]. For a discharge with hundreds of microns gap length, the electric field is usually two orders of magnitudes lower and the discharge is sustained by ion-impact secondary electron emission at the cathode. With the presence of the surface protrusion on the electrode, the electric field can be enhanced on the protrusion tip and the local electric field enhancement factor β could be larger than 10^2, depending on the protrusion irregularity [24]. This could result in the breakdown mode transition from the secondary electron emission to the field emission [21]. However, with a regular protrusion or a smooth

Manuscript received September 2, 2018; revised October 13, 2018; accepted October 21, 2018. Date of publication November 12, 2018; date of current version May 8, 2019. This work was supported in part by Air Force Office of Scientific Research (AFOSR) under Grant FA9550-18-1-0062, in part by the U.S. Department of Energy Plasma Science Center under Grant DE-SC0001939, and in part by MSU Strategic Partnership Grant. The work of P. Zhang was also supported by the AFOSR Young Investigator Program under Award FA9550-18-1-0061. The review of this paper was arranged by Senior Editor S. J. Gitomer. *(Corresponding author: Yangyang Fu.)*

Y. Fu and J. P. Verboncoeur are with the Department of Computational Mathematics Science and Engineering, Michigan State University, East Lansing, MI 48824 USA, and also with the Department of Electrical and Computer Engineering, Michigan State University, East Lansing, MI 48824 USA (e-mail: fuyangya@egr.msu.edu; johnv@egr.msu.edu).

J. Krek is with the Department of Computational Mathematics Science and Engineering, Michigan State University, East Lansing, MI 48824 USA (e-mail: krek@egr.msu.edu).

P. Zhang is with the Department of Electrical Engineering, Michigan State University, East Lansing, MI 48824 USA (e-mail: pz@egr.msu.edu).

Color versions of one or more of the figures in this paper are available online at http://ieeexplore.ieee.org.

Digital Object Identifier 10.1109/TPS.2018.2878011

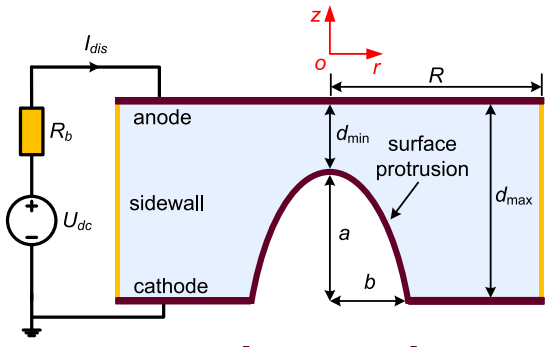

Fig. 1. Schematic of the discharge model. A dc voltage source applied to a microgap with a hemiellipsoidal protrusion on the cathode surface through a ballast resistor.

tip protrusion, i.e., hemiellipsoidal or hemispherical protrusions, the electric field enhancement might be less significant, which will not necessarily lead to the field emission [15]. Even though the transition from secondary electron emission to the field emission may not happen, an introduced protrusion can still change the flux of the charged particles in this regime that might also have a significant impact on the breakdown characteristics in the microgap [25].

Fu *et al.* [15], [25] investigated the impacts of the electrode surface protrusion on breakdown characteristics in microgaps. This paper gives a more detailed and complete study of the parameter dependence. More specifically, the field enhancement across the gap and the cathode current distribution characteristics are presented to confirm the dominant impact parameters. The breakdown voltage is quantified based on voltage–current characteristics using a 2-D fluid model. The geometry of the surface protrusion is assumed to be hemiellipsoidal and hemispherical. By adjusting the protrusion parameters, the effects of the protrusion size, protrusion aspect ratio, and the discharge polarity on the breakdown properties are studied. By sweeping the gas pressure in a focused range, Paschen's curves in microgaps with a surface protrusion on the electrodes are also obtained.

In Section II, the model description including the schematic of the microgap, mathematical equation, and boundary condition is given. In Section III, the results on the effect of the protrusion geometry, Paschen's curve, and the effect of the discharge polarity are presented. Finally, the conclusion is given in Section IV.

II. Model Description

A. Schematic of the Microgap

The schematic of the microgap is shown in Fig. 1. A dc voltage $U_{\rm dc}$ is applied to the anode through a ballast resistor $R_{\rm b} = 100\ {\rm k}\Omega$, while the cathode is grounded. $I_{\rm dis}$ is the discharge current. The microgap consists of two plane–parallel circular electrodes with a single hemiellipsoidal protrusion on the cathode. The geometry of the protrusion is characterized by the protrusion height a and the radius b, and the protrusion will be hemispherical if $a = b$. The electrode protrusion results in the minimum distance $d_{\rm min}$ from the protrusion tip to the opposite anode. The maximum gap distance $d_{\rm max}$ is between the flat surface of the cathode and the anode. The coordinates are in the rz plane, and R is the electrode radius. Argon gas at room temperature 300 K (0.026 eV) is chosen as the working gas. The gap distance ranges from 50 to 500 μm, and the protrusion height ranges from 25 to 450 μm.

In the cases studied, the gap voltage is no larger than 200 V. With the gap distance ranging from 50 to 500 μm and the field enhancement less than 10 [see Fig. 7(b)], the maximum electric field is on the order of 10^7 V/m while the space charge is not important. Therefore, field emission can be ignored since the maximum effective electric field is much smaller than the field emission threshold (10^9 V/m) [2], [20]–[22]. The discharge in this regime is still dominated by ion-impact secondary electron emission at the cathode. By adjusting the parameters including $d_{\rm min}$, $d_{\rm max}$, a, b, and R, the effects of the protrusion height, protrusion radius, as well as the aspect ratios can be investigated, respectively.

B. Mathematical Equation

The fluid model has been widely used and conducted successfully in high-pressure discharges where the drift–diffusion approximation is valid [26]. The mathematical equations of the fluid model include the species continuity equation, electron energy conservation equation, and Poisson's equation, which are solved self-consistently [27]–[30].

For each species j in the discharge, the time evolution of density is described by the continuity equation

$$\frac{\partial n_j}{\partial t} + \nabla \cdot \vec{\Gamma}_j = S_j \tag{1}$$

where n_j, $\vec{\Gamma}_j$, and S_j are the density, the flux, and the source term of species j, respectively. The species j could be electrons, ions, or excited atoms. The flux $\vec{\Gamma}_j$ is given as

$$\vec{\Gamma}_j = {\rm sgn}(q_j) n_j \mu_j \vec{E} - D_j \nabla n_j \tag{2}$$

where q_j is the charge of species j, $\vec{E}$ is the electric field, μ_j is the mobility, and D_j is the diffusion coefficient for the species j. ${\rm sgn}(q_j)$ is $+1$, -1, or 0 for positive ion, electron, or neutral species, respectively. The general form of the source term S_j is expressed as

$$S_j = \sum_k^N \sum_i k_{ik} n_k \tag{3}$$

where k_{ik} is the ith reaction rate coefficient with the kth species, and N is the number of species related to the ith reaction.

The electron energy transport equation is usually expressed with the quasi-thermal equilibrium model [31]

$$\frac{\partial n_\varepsilon}{\partial t} + \nabla \cdot \left(-\frac{5}{3} \mu_e \vec{E} n_\varepsilon - \frac{5}{3} D_e \nabla n_\varepsilon \right) = S_\varepsilon \tag{4}$$

where n_ε is the electron energy density. The source term for electron energy is given as

$$S_\varepsilon = -q_e \vec{\Gamma}_e \cdot \vec{E} - \sum_k \sum_i \Delta\varepsilon_i k_{ik} n_k \tag{5}$$

where $\Delta\varepsilon_i$ is the energy loss in the ith reaction.

The Poisson's equation is given as

$$\nabla^2\phi = -\frac{1}{\varepsilon_0\varepsilon_r}\sum_j q_j n_j \text{ and } \vec{E} = -\nabla\phi \tag{6}$$

where ϕ is the electric potential, ε_0 is the vacuum permittivity, and ε_r is the relative permittivity of the working gas.

C. Boundary Condition

The equations were solved in a cylindrical domain (r and z). The symmetry conditions were assumed at the axis ($r = 0$)

$$\vec{\Gamma}_j \cdot \vec{n} = 0, \quad \vec{\Gamma}_\varepsilon \cdot \vec{n} = 0, \quad \vec{E} \cdot \vec{n} = 0 \tag{7}$$

where $\vec{n}$ is the normal unit vector pointing toward the wall. The boundary condition for the ions at an absorbing electrode wall is

$$\vec{\Gamma}_i \cdot \vec{n} = \frac{1}{2}v_{\text{th}}^i n_i + \delta_i \mu_i \vec{E} \cdot \vec{n} n_i \tag{8}$$

where v_{th}^i is the thermal velocity of the ions and δ_i is set to 1 if the electric field is directed toward the wall, or 0 otherwise. For the electrons and electron energy flux, the boundary conditions are given as [32]

$$\vec{\Gamma}_e \cdot \vec{n} = \frac{1}{2}v_{\text{th}}^e n_e - \delta_e \gamma \vec{\Gamma}_i \cdot \vec{n} \tag{9}$$

$$\vec{\Gamma}_\varepsilon \cdot \vec{n} = \frac{5}{6}v_{\text{th}}^e n_\varepsilon - \delta_e \tilde{\varepsilon}_e \gamma \vec{\Gamma}_i \cdot \vec{n} \tag{10}$$

where v_{th}^e is the electron thermal velocity and $\delta_e = 1$ if $\vec{\Gamma}_e \cdot \vec{n} > 0$, or $\delta_e = 0$ otherwise, $\tilde{\varepsilon}_e$ is the mean energy of the emitted electrons, and γ is the secondary electron emission coefficient, which is 0.1 at the cathode and 0 at other walls [33], [34].

At the side wall boundary ($r = R$), the following conditions are specified:

$$\vec{E} \cdot \vec{n} = \sigma_s/\varepsilon_0 \tag{11}$$

$$\frac{d\sigma_s}{dt} = q_e(\vec{\Gamma}_i - \vec{\Gamma}_e) \cdot \vec{n} \tag{12}$$

where σ_s is the surface charge density. The boundary conditions for the potential ϕ at the anode and the cathode are $\phi(r, 0) = 0$ and $\phi(r, d_{\max}) = U_{\text{dc}} - I_{\text{dis}} \cdot R_b$, respectively. Although a more accurate description of the discharge may require kinetic treatment of electrons, the fluid model can still capture the transition from the Townsend regime to glow discharge regime, which can be employed to understand the qualitative trends of the breakdown curves with the perturbation of the protrusion geometry [35], [36].

III. Results and Discussion

The breakdown voltage was quantified according to the obtained voltage–current characteristic curves, which include Geiger–Müller regime, Townsend discharge regime, and subnormal glow discharge regime. Note that unlike the slow glow breakdowns or the fast streamer breakdowns in other situations, the breakdown, here, is quantified at the transition between the Townsend regime and the subnormal glow regime.

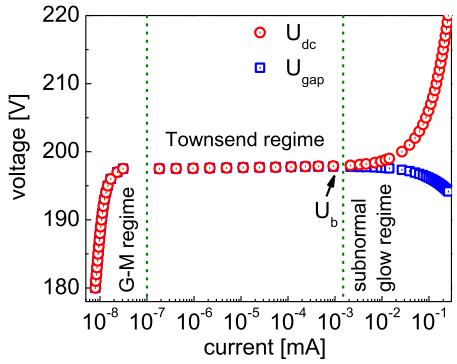

Fig. 2. Voltage–current characteristics for a microgap with $a = b = 100$ μm, $R = 500$ μm, and $d_{\max} = 500$ μm at atmospheric pressure. Reproduced from [15], with the permission of AIP Publishing.

By gradually increasing the applied voltage U_{dc} in small steps in a sequence of simulations, the voltage–current characteristics can be obtained. Fig. 2 shows a typical voltage–current curve with a surface protrusion on the cathode and different discharge regimes are delimited by current intervals. It can be seen that the curve is relatively flat in Townsend regime while the applied voltage U_{dc} and the gap voltage U_{gap} departure from each other in the subnormal glow regime. The critical point of the gas breakdown is quantified when the discharge enters the subnormal glow regime with a negative differential resistance, as shown in Fig. 2. The breakdown voltage is defined as the maximum gap voltage when the discharge transits from the Townsend regime to the subnormal glow regime [37], [38]. Without defining a threshold of the magnitude of the breakdown current, the breakdown voltage can be identified with a very small uncertainty (less than 0.5 V).

A. Effect of the Protrusion Geometry

As is known, the geometry of the microgap and the surface protrusion can both have an impact on the breakdown voltage. We first assume a relatively small protrusion ($a \leq 100$ μm) on the cathode and set $d_{\max} = R = 500$ μm at atmospheric pressure, focusing on the effect of the protrusion geometry. By changing the protrusion geometry parameters a and b, the effects of the protrusion height and its aspect ratio are studied, as shown in Fig. 3.

Fig. 3(a) presents the comparison of the effects of protrusion size and aspect ratio on the breakdown voltage. Increasing the aspect ratio a/b from 0.5 to 2.0 with $a = 100$ μm, the breakdown voltage shows little changes, less than 3 V. Keeping the aspect ratio fixed at 1, i.e., $a = b$, as the size of the protrusion increases, the breakdown voltage decreases significantly from 220 to 197 V. The breakdown voltage is more sensitive to the protrusion size than the aspect ratio. In this atmospheric-pressure regime, the breakdown regime is on the right branch of Paschen's curve and the breakdown behavior is mainly determined by the effective gap distance (the shortest distance $d_{\min}$). When the protrusion size is increased, $d_{\min}$ becomes smaller and then the breakdown will be achieved easier, which results in the decrease in the

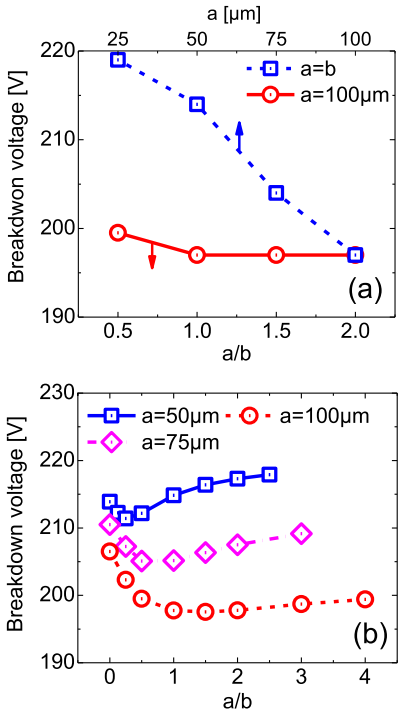

Fig. 3. Effect of the protrusion geometry on breakdown voltages in microgap at atmospheric pressure. (a) Comparing the effects of the protrusion size and aspect ratio. (b) Breakdown voltage versus the aspect ratio with protrusion height fixed at different values. Reproduced from [15], with the permission of AIP Publishing.

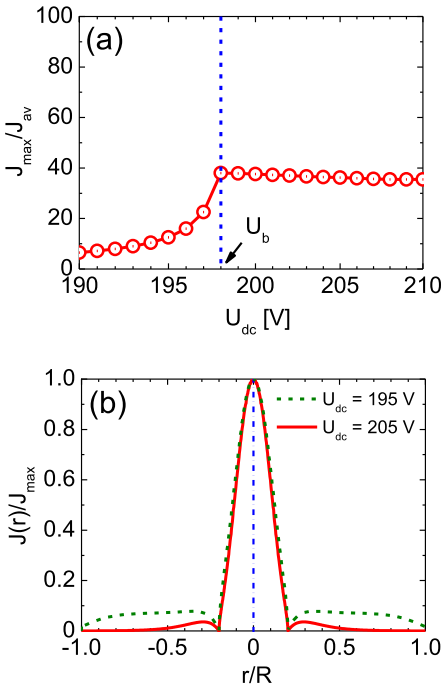

Fig. 4. (a) Ratio between the maximum current density $J_{\max}$ and the average current density J_{av} versus the applied voltage U_{dc}. (b) Normalized current density distributions in the radial direction with applied voltage at 195 and 205 V, respectively. In the simulation, $a = b = 100$ μm, $R = 500$ μm, and $d_{\max} = 500$ μm.

breakdown voltage. On the other hand, increasing the aspect ratio, though it enhances the electric field, the enhancement factor is not sufficiently high. Therefore, the decrease in the breakdown voltage is small.

If the protrusion aspect ratio varies in a wider range (a/b ranges from 0 to 4) with the protrusion height fixed at 50, 75, and 100 μm, respectively, the breakdown voltage as a function of a/b shows a minimum, as shown in Fig. 3(b). This behavior is very different from the expectation that the breakdown voltage will decrease if the protrusion becomes sharper. In the following, the cathode current emission is presented to explain this phenomenon.

Take the case $a = b = 100$ μm (corresponds to Fig. 2), for example, the characteristics of the cathode current emission is shown in Fig. 4. Fig. 4(a) shows the ratio between the maximum current density $J_{\max}$ and the average current density J_{av} versus the applied voltage U_{dc}. It is observed that as the applied voltage increases, the current ratio $J_{\max}/J_{\text{av}}$ reaches a turning point. Correspondingly, the breakdown voltage, here, is recognized at 198 V, which is the same as the one identified from the voltage–current curves in Fig. 2. Fig. 4(b) shows the normalized current density distributions in the radial direction with applied voltage at 195 V (before breakdown) and 205 V (after breakdown), respectively. For both cases, the current density distribution is distorted and becomes nonmonotonic in the radial direction due to the surface protrusion. The current density drops to zero at the corner between the (perfectly conducting) protrusion and the substrate, which is very different from the plane–parallel cases [33]. The maximum current density is on the protrusion tip which is much larger (orders higher) than the current density on the substrate, which is almost ignorable. The general effect of the protrusion is increasing the current density on the tip whereas decreasing the effective emission area. Therefore, a sharper protrusion will not necessarily increase the total cathode emission current or result in a lower breakdown voltage, since the current density enhancement competes with the effective emission area under different conditions. With the protrusion height fixed, when the protrusion aspect ratio is small (flat protrusion), increasing a/b can increase the current density enhancement, which lowers the breakdown voltage; however, when the aspect ratio is large (sharp protrusion), increasing a/b can decrease the effective emission area, which requires a high voltage to increase the ionization frequency to ignite the breakdown. This explains the lowest breakdown point in Fig. 3(b) and confirms the effect of the surface protrusion geometry on the breakdown voltage is not monotonic.

B. Paschen's Curve

In order to show the effect of the surface protrusion on Paschen's curve, three cases with and without surface protrusion are considered, as shown in Fig. 5(a). Cases 1 and 2 are the plane–parallel electrodes with a gap distance at 50 and 500 μm, which span the minimum and the maximum gap distance in case 3 with the presence of a surface protrusion ($a = 450$ μm and $b = 200$ μm) on the cathode. The microgap radius R is set at 1000 μm to exclude the effect of the side wall. Fig. 5(b) shows the obtained Paschen's curve for all

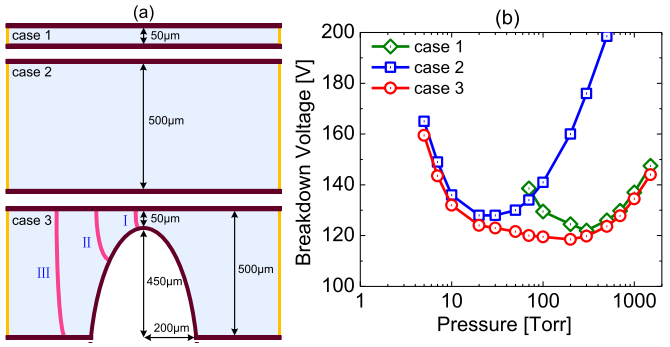

Fig. 5. (a) Cases 1 and 2: plane–parallel electrode with a gap distance at 50 μm (short gap) and 500 μm (long gap), respectively; case 3: plane–parallel microgap with a hemiellipsoidal protrusion ($a = 450$ μm and $b = 200$ μm) on the cathode. (b) Calculated Paschen's curve with $R = 1000$ μm, data from [25].

cases. It can be seen that in the shorter gap (case 1) Paschen's curve stays in a high-pressure regime, whereas in the longer gap (case 2) it is located in a low-pressure regime. In case 3, the cathode surface protrusion results in a combined Paschen's curve, which transits from long-gap behavior at low pressure to short-gap behavior at high pressure, keeping the breakdown voltage relatively low in a wide range of gas pressure.

This is due to the migration of the major discharge path inside the gap as the gas pressure varies. As is shown in Fig. 5(a) for case 3, at high pressures, the breakdown occurs along the shortest path which is between the protrusion tip and the opposite electrode. As the pressure decreases, the mean free path λ of electron–neutral collision becomes larger and the breakdown tends to automatically optimize its path which is proportional to λ. In such a way, as the pressure decreases, the discharge path automatically moves from the top of the protrusion (path I) to its side surface (path II) and then to the cathode substrate (path III). The simulation results of the discharge path migration can be found in [25]. Therefore, at high pressures, the breakdown property is mainly determined by the shortest gap distance $d_{\min}$, while at low pressures it is mainly determined by the longest gap distance $d_{\max}$. As for the combined Paschen's curve, the corresponding right branch (at high pressure) is close to the 50-μm plane–parallel gap (case 1), and the corresponding left branch is similar to the 500-μm plane–parallel gap (case 2). The most interesting phenomena are that the surface protrusion makes Paschen's curve flattened and results in relatively low breakdown voltages across a wide pressure range.

Fig. 6 shows the effect of the protrusion radius on Paschen's curve with $d_{\min} = 50$ μm and the impact factors on the breakdowns. Increasing the protrusion radius only show impact on the left branch Paschen's curve whereas less impact on the right branch, as shown in Fig. 6(a). This phenomenon can be explained based on two impact factors: the vacuum electric field enhancement, as shown in Fig. 6(b), and the effective cathode emission areas, as shown in Fig. 6(c). As for the right branch, the breakdown occurs along the path I [see case 3 in Fig. 5(a)] and the breakdown voltage is mainly determined by $d_{\min}$, which is fixed. On the other hand, the maximum electric field enhancement from the protrusion tip to the anode

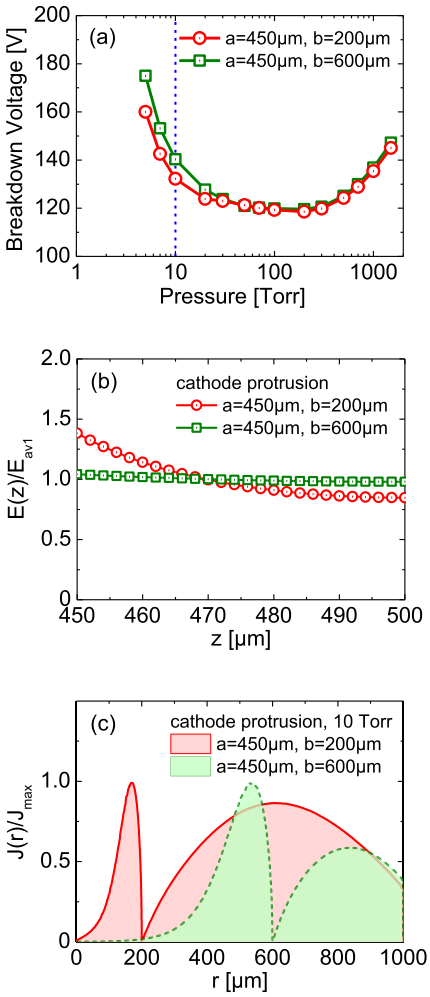

Fig. 6. (a) Effect of the cathode protrusion radius on Paschen's curve. (b) Vacuum electric field enhancement from the cathode protrusion tip ($z = 450$ μm) to the opposite anode ($z = 500$ μm) with different protrusion radii. (c) Normalized cathode current distribution with different protrusion radii at 10 torr.

is less than 1.5, which is not severe here. Note that E_{av1} is defined as $E_{\text{av1}} = U/d_{\min}$ since the discharge is mainly affected by the electric field strength in the tip region. The electric field is quite uniform along the axis and the electric field difference has little impact. Therefore, the breakdown voltage difference caused by different protrusion radii is less distinguishable on the right branch.

As for the left branch, the breakdown chooses longer paths (paths II or III) and the breakdown is largely influenced by the effective cathode current emission area. As is shown in Fig. 6(c), for the case (10 torr) on the left branch, the current density peak location shifts from the protrusion tip [see Fig. 4(b) at atmospheric pressure] to the side of the protrusion or the cathode substrate at low pressures. It is observed that the larger the protrusion radius is, the smaller is the effective cathode emission area, which results in higher breakdown voltages on the left branch of Paschen's curve. Note that even though a cathode protrusion with a larger radius could result in lower breakdown voltages at high pressures

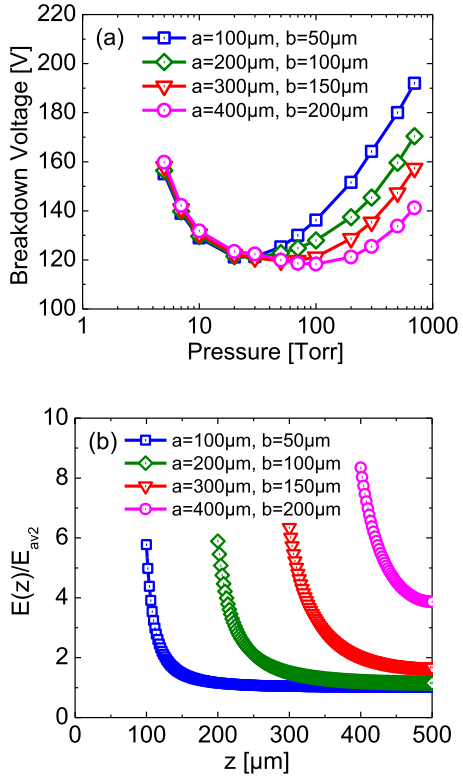

Fig. 7. (a) Effect of the cathode protrusion height on Paschen's curve. (b) Vacuum electric field enhancement from the cathode protrusion tip to the opposite anode with a fixed aspect ratio.

[see Fig. 3(b)], to obtain a flattened breakdown curve, a broader protrusion is not desirable at low pressures when the effective cathode emission area has a strong effect on the breakdown processes.

The effect of the protrusion height on Paschen's curve is shown in Fig. 7(a) with the aspect ratio fixed at $a/b = 2$. The protrusion height has a significant impact on the right branch of Paschen's curve but less impact on the left branch. This is also consistent with our previous analysis. On the right branch (at high pressure), the breakdown voltage is dominated by the shortest gap distance $d_{\min}$ ($d_{\min} = d_{\max} - a$). The larger the protrusion height is, the smaller is $d_{\min}$, which leads to lower breakdown voltages. The vacuum electric field enhancements are also shown in Fig. 7(b) and to avoid the complication caused by the changing $d_{\min}$, E_{av2} is defined as $E_{\text{av2}} = U/d_{\max}$ for comparison. Since the aspect ratio of the protrusion is fixed, the field enhancement is roughly the same when the protrusion height is small, where it is further enhanced when the protrusion tip approaches the facing electrode. Comparing the shortest gap distance, the difference in the field enhancement is less important here. It is worth noting that even though the field enhancements are not exactly the same, their impacts on the breakdown tendency are consistent, i.e., a larger field enhancement leads to a lower breakdown voltage.

C. Effect of the Discharge Polarity

In order to show the effect of the surface protrusion with different discharge polarities, the aspect ratio is set to $a/b = 2$.

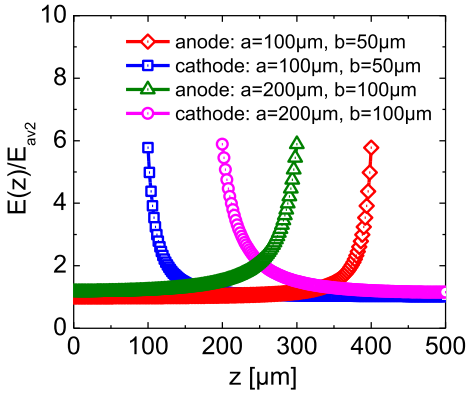

Fig. 8. Vacuum electric field enhancement with the presence of the surface protrusion with different sizes on the cathode ($z = 0$ μm) and the anode surface ($z = 500$ μm). The aspect ratio of the protrusions is fixed at $a/b = 2$.

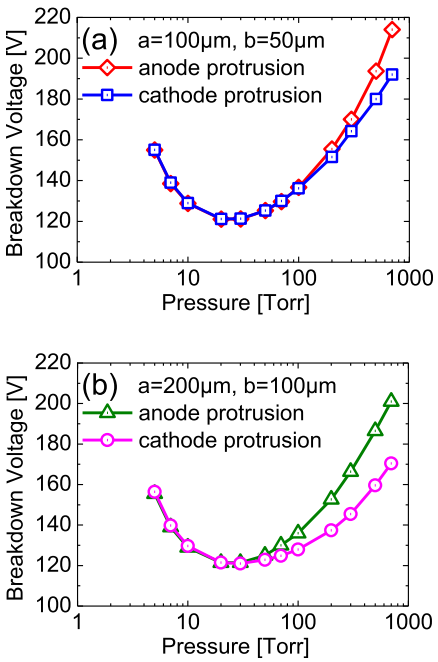

Fig. 9. Effect of discharge polarity on Paschen's curve, data from [25]. (a) Protrusion parameter: $a = 100$ μm and $b = 50$ μm. (b) Protrusion parameter: $a = 200$ μm and $b = 100$ μm.

In such a way, the protrusion height can be increased with maintaining the field enhancement roughly the same.

Fig. 8 shows the vacuum electric field enhancement in the axial direction with the surface protrusion on the anode and the cathode and for two different heights. The maximum electric fields near the protrusion tip are almost the same, approximating to six times the averaged electric field. However, the field enhancements are opposite at the cathode and the anode when the protrusion polarity is different. That is to say, the electric field is enhanced at the anode with an anode protrusion while it is enhanced near the cathode with a cathode protrusion. Therefore, the effect of the discharge polarity could be mainly caused by different profiles of the electric field, which might change the ion flux and the cathode emission processes.

Fig. 9 shows the obtained Paschen's curve with a surface protrusion on the anode and the cathode. In Fig. 9(a), the protrusion sizes are $a = 100$ μm and $b = 50$ μm, and in Fig. 9(b),

(a)

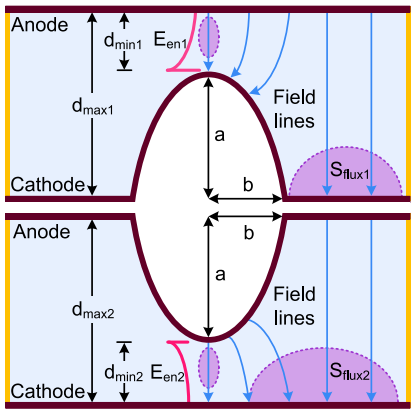

(b)

Pressure / Polarity	High pressure (Short path)	Low pressure (Long path)
Anode protrusion	Diverging E field line Smaller cathode E_{en}	Converging E field line Larger cathode S_{flux}
Cathode protrusion	Converging E field line Larger cathode E_{en}	Diverging E field line Smaller cathode S_{flux}

Fig. 10. Illustration of the effect of surface protrusions on the gas breakdown. (a) Summary of the key parameters: $d_{\min 1}$ and $d_{\min 2}$ are the shortest gap distances, $d_{\max 1}$ and $d_{\max 2}$ are the longest gap distances, $E_{\text{en}1}$ and $E_{\text{en}2}$ are the electric field enhancements, and $S_{\text{flux}1}$ and $S_{\text{flux}2}$ are the effective cathode emission areas [25]. (b) Key factors listed for different situations. Note that the diverging and the converging E-fields are with respect to the cathode surface area where breakdown occurs.

the protrusion sizes are $a = 200$ μm and $b = 100$ μm. It can be seen that the effect of the protrusion height on Paschen's curve is more distinguishable on its right branch and almost negligible on its left branch. Similarly, this phenomenon can be explained as earlier, but the difference of the cathode electric field enhancement has to be considered.

As it was aforementioned, at high pressure (on the right branch), the discharge usually undergoes a short path and mainly occurs between the protrusion tip and the opposite electrode. With a cathode protrusion, the electric field is enhanced near the cathode and then local ionization and the ion-impact flux will be more efficient, which results in lower breakdown voltages than that with the anode protrusion. On the other hand, at high pressures, the discharge occurs in the center of the electrodes, where the electric field lines [see Fig. 10(a)] toward the cathode center are converging with a cathode protrusion, while are diverging with an anode protrusion. This also indicates that the breakdown voltage with a cathode protrusion will be lower than that with an anode protrusion. On the left branch (at low pressure), the breakdown behaviors are mainly determined by the longest gap distance $d_{\max}$, which is fixed at 500 μm for all the cases in Fig. 9. Thus, the breakdown curves overlap on the left branch of Paschen's curve.

Fig. 10 shows the key factors impacting on the breakdown characteristics with the surface protrusion on the cathode and the anode. For a given microgap with different polarities, the key parameters include the shortest gap distance ($d_{\min 1}$ and $d_{\min 2}$), the longest gap distance ($d_{\max 1}$ and $d_{\max 2}$), the electric field enhancement ($E_{\text{en}1}$ and $E_{\text{en}2}$), and the effective cathode emission areas ($S_{\text{flux}1}$ and $S_{\text{flux}2}$), which are illustrated in Fig. 10(a). Which parameters come into play depends on the gas pressure and the discharge polarity, as is shown in Fig. 10(b). At high pressures, $d_{\min 1}$ and $d_{\min 2}$ are the key parameters for the breakdown. $E_{\text{en}1}$ and $E_{\text{en}2}$ should be considered correspondingly when the polarity is changed. At low pressures, $d_{\max 1}$ and $d_{\max 2}$ are the key parameters for the breakdown. $S_{\text{flux}1}$ and $S_{\text{flux}2}$ should be also considered when the polarity is changed. Generally, when the geometry sizes are the same ($d_{\min 1} = d_{\min 2}$ and $d_{\max 1} = d_{\max 2}$), due to different polarities ($E_{\text{en}1} > E_{\text{en}2}$ and $S_{\text{flux}1} < S_{\text{flux}2}$), a larger field enhancement near the cathode or a larger effective cathode emission area will lead to lower breakdown voltages. In addition, the convergence and the divergence of the electric field also have an impact on the charge fluxes and the breakdown voltages, shown in Fig. 10(a). For the gas breakdown at high pressures, the converging electric field lines with a cathode protrusion will results in a lower breakdown voltage compared to that with an anode protrusion having the diverging field lines. Note that this impact tendency on the breakdown voltage is consistent with the electric field enhancement.

IV. Conclusion

The gas breakdown characteristics in microgaps with a surface protrusion on the electrode are quantified using the 2-D fluid model. More detailed discussion of the field enhancement and the cathode current distributions affected by the protrusion geometries is provided, which gives a more complete study of the parameter dependence. The effects of the protrusion geometry parameters, such as protrusion size and its aspect ratio, are investigated. It is found that the breakdown voltage is more sensitive to the protrusion size than its aspect ratio, and the impact of the aspect ratio on the breakdown voltage is non-monotonic, depending on the competition between the current density enhancement and the effective cathode emission area. The surface protrusion on the electrode results in a combined Paschen's curve, which shows the breakdown transition from long-gap behavior at low pressure to short-gap behavior at high pressure, keeping the breakdown voltage relatively low in a wide range of gas pressure. The key parameters for the impact of the surface protrusion on the shape of Paschen's curve are elucidated. This paper provides insights into the design of microgaps with controlled breakdown voltage by shaping the electrode with engineered morphology.

References

[1] F. Iza, J. K. Lee, and M. G. Kong, "Electron kinetics in radio-frequency atmospheric-pressure microplasmas," *Phys. Rev. Lett.*, vol. 99, no. 7, p. 075004, 2007.

[2] D. B. Go and D. A. Pohlman, "A mathematical model of the modified Paschen's curve for breakdown in microscale gaps," *J. Appl. Phys.*, vol. 107, no. 10, p. 103303, 2010.

[3] K. H. Schoenbach and W. Zhu, "High-pressure microdischarges: Sources of ultraviolet radiation," *IEEE J. Quantum Electron.*, vol. 48, no. 6, pp. 768–782, Jun. 2012.

[4] M. Radmilović-Radjenović, Š. Matejčik, M. Klas, and B. Radjenović, "The role of the field emission effect in direct-current argon discharges for the gaps ranging from 1 to 100 μm," *J. Phys. D, Appl. Phys.*, vol. 46, no. 1, p. 015302, 2013.

[5] S. Wu, F. Wu, X. Liu, W. Chen, C. Liu, and C. Zhang, "Investigation on the characteristics of an atmospheric-pressure microplasma plume confined inside a long capillary tube," *Plasma Sci. Technol.*, vol. 20, no. 10, p. 105402, 2018.

[6] F. Paschen, "Ueber die zum Funkenübergang in luft, wasserstoff und Kohlensäure bei verschiedenen drucken erforderliche potentialdifferenz," *Ann. Phys.*, vol. 273, no. 5, pp. 69–96, 1889.

[7] V. A. Lisovskiy, S. D. Yakovin, and V. D. Yegorenkov, "Low-pressure gas breakdown in uniform DC electric field," *J. Phys. D, Appl. Phys.*, vol. 33, no. 21, pp. 2722–2723, 2000.

[8] R. Tirumala and D. B. Go, "An analytical formulation for the modified Paschen's curve," *Appl. Phys. Lett.*, vol. 97, no. 15, p. 151502, 2010.

[9] V. F. Tarasenko *et al.*, "Influence of electrode spacing and gas pressure on parameters of a runaway electron beam generating during the nanosecond breakdown in SF6 and nitrogen," *High Volt.*, vol. 2, no. 2, pp. 49–55, Jun. 2017.

[10] Y. Fu, S. Yang, X. Zou, H. Luo, and X. Wang, "Intersection of Paschen's curves for argon," *Phys. Plasmas*, vol. 23, no. 9, p. 093509, 2016.

[11] Y. Fu, S. Yang, X. Zou, H. Luo, and X. Wang, "Effect of distribution of electric field on low-pressure gas breakdown," *Phys. Plasmas*, vol. 24, no. 2, p. 023508, 2017.

[12] N. Bhattacharjee, A. Urrios, S. Kang, and A. Folch, "The upcoming 3D-printing revolution in microfluidics," *Lab Chip*, vol. 16, no. 10, pp. 1720–1742, 2016.

[13] S. Martínez-Jarquín, A. Moreno-Pedraza, H. Guillèn-Alonso, and R. Winkler, "Template for 3D printing a low-temperature plasma probe," *Anal. Chem.*, vol. 88, no. 14, pp. 6976–6980, 2016.

[14] J. A. Buendia and A. Venkattraman, "Field enhancement factor dependence on electric field and implications on microscale gas breakdown: Theory and experimental interpretation," *Europhys. Lett.*, vol. 112, no. 5, 2015, Art. no. 55002.

[15] Y. Fu, P. Zhang, and J. P. Verboncoeur, "Gas breakdown in atmospheric pressure microgaps with a surface protrusion on the cathode," *Appl. Phys. Lett.*, vol. 112, no. 25, p. 254102, 2018.

[16] A. Peschot, N. Bonifaci, O. Lesaint, C. Valadares, and C. Poulain, "Deviations from the Paschen's law at short gap distances from 100 nm to 10 μm in air and nitrogen," *Appl. Phys. Lett.*, vol. 105, no. 12, p. 123109, 2014.

[17] Y. Fu, P. Zhang, J. P. Verboncoeur, A. J. Christlieb, and X. Wang, "Effect of surface protrusion on plasma sheath properties in atmospheric microdischarges," *Phys. Plasmas*, vol. 25, no. 1, p. 013530, 2018.

[18] G. Meng, Y. Cheng, X. Gao, K. Wang, C. Dong, and B. Zhu, "*In-situ* optical observation of dynamic breakdown process across microgaps at atmospheric pressure," *IEEE Trans. Dielectr. Elect. Insul.*, vol. 25, no. 4, pp. 1502–1507, Aug. 2018.

[19] G. Meng *et al.*, "Demonstration of field emission driven microscale gas breakdown for pulsed voltages using *in-situ* optical imaging," *Phys. Plasmas*, vol. 25, no. 8, p. 082116, 2018.

[20] D. Levko and L. L. Raja, "Breakdown of atmospheric pressure microgaps at high excitation frequencies," *J. Appl. Phys.*, vol. 117, no. 17, p. 173303, 2015.

[21] Y. Fu, J. Krek, P. Zhang, and J. P. Verboncoeur, "Evaluating microgap breakdown mode transition with electric field non-uniformity," *Plasma Sources Sci. Technol.*, vol. 27, no. 9, p. 095014, 2018.

[22] A. M. Loveless and A. L. Garner, "Generalization of microdischarge scaling laws for all gases at atmospheric pressure," *IEEE Trans. Plasma Sci.*, vol. 45, no. 4, pp. 574–583, Apr. 2017.

[23] M. Radmilović-Radjenović and B. Radjenović, "Theoretical study of the electron field emission phenomena in the generation of a micrometer scale discharge," *Plasma Sources Sci. Technol.*, vol. 17, no. 2, p. 024005, May 2008.

[24] A. Semnani, A. Venkattraman, A. A. Alexeenko, and D. Peroulis, "Pre-breakdown evaluation of gas discharge mechanisms in microgaps," *Appl. Phys. Lett.*, vol. 102, no. 17, p. 174102, 2013.

[25] Y. Fu, P. Zhang, and J. P. Verboncoeur, "Paschen's curve in microgaps with an electrode surface protrusion," *Appl. Phys. Lett.*, vol. 113, no. 5, p. 054102, 2018.

[26] S. W. Hwang, H.-J. Lee, and H. J. Lee, "Effect of electron Monte Carlo collisions on a hybrid simulation of a low-pressure capacitively coupled plasma," *Plasma Sour. Sci. Technol.*, vol. 23, no. 14, p. 065040, Sep. 2014.

[27] G. J. M. Hagelaar and L. C. Pitchford, "Solving the Boltzmann equation to obtain electron transport coefficients and rate coefficients for fluid models," *Plasma Sour. Sci. Technol.*, vol. 14, no. 4, p. 722, 2005.

[28] S. He, P. Wang, J. Ha, B. Zhang, Z. Zhang, and Q. Li, "Effects of discharge parameters on the micro-hollow cathode sustained glow discharge," *Plasma Sci. Technol.*, vol. 20, no. 5, p. 054006, 2018.

[29] Y. Fu, H. Luo, X. Zou, and X. Wang, "Research on similarity law of glow discharge in argon at low pressure by numerical simulation," *IEEE Trans. Plasma Sci.*, vol. 42, no. 6, pp. 1544–1551, Jun. 2014.

[30] Y. Fu, H. Luo, X. Zou, and X. Wang, "Validity of the similarity law for the glow discharges in non-plane-parallel gaps," *Plasma Sources Sci. Technol.*, vol. 23, no. 6, p. 065035, 2014.

[31] D. B. Graves, "Fluid model simulations of a 13.56-MHz RF discharge: Time and space dependence of rates of electron impact excitation," *J. Appl. Phys.*, vol. 62, no. 1, p. 88, 1987.

[32] E. A. Bogdanov, V. I. Demidov, A. A. Kudryavtsev, and A. I. Saifutdinov, "Is the negative glow plasma of a direct current glow discharge negatively charged?" *Phys. Plasmas*, vol. 22, no. 2, p. 024501, 2015.

[33] Y. P. Raizer, *Gas Discharge Physics*. Berlin, Germany: Springer, 1991.

[34] A. V. Phelps and Z. L. Petrovic, "Cold-cathode discharges and breakdown in argon: Surface and gas phase production of secondary electrons," *Plasma Sources Sci. Technol.*, vol. 8, no. 3, p. R21, 1999.

[35] R. R. Arslanbekov and V. I. Kolobov, "Two-dimensional simulations of the transition from Townsend to glow discharge and subnormal oscillations," *J. Phys. D, Appl. Phys.*, vol. 36, no. 23, pp. 2986–2994, 2003.

[36] I. Rafatov and C. Yesil, "Transition from homogeneous stationary to oscillating state in planar gas discharge–semiconductor system in nitrogen: Effect of fluid modelling approach," *Phys. Plasmas*, vol. 25, no. 8, p. 082107, 2018.

[37] A. M. Bilici, J. R. Haase, C. R. Boyle, D. B. Go, and R. M. Sankaran, "A smooth transition from field emission to a self-sustained plasma in microscale electrode gaps at atmospheric pressure," *J. Appl. Phys.*, vol. 119, no. 22, p. 223301, 2016.

[38] J. T. Gudmundsson and A. Hecimovic, "Foundations of DC plasma sources," *Plasma Sources Sci. Technol.*, vol. 26, no. 12, p. 123001, 2017.

Yangyang Fu (M'16) received the bachelor's degree in electrical engineering from Shanghai Jiao Tong University, Shanghai, China, in 2010, and the Ph.D. degree in electrical engineering from Tsinghua University, Beijing, China, in 2015, respectively.

He is currently a Research Associate with the Department of Computational Mathematics Science and Engineering, Michigan State University, East Lansing, MI, USA. His current research interests include microdischarges, gas breakdown, low-temperature plasma scaling laws, and plasma simulation methods.

Dr. Fu was a Committee Member of the 2018 ICOPS NPSS Outstanding Student Paper Award. He was a recipient of the Outstanding Reviewer Award for *Plasma Sources Science and Technology* from the Institute of Physics in 2017, the Excellent Dissertation Award (1st Place), the Academic Star Award, the Excellent Graduate Award from Tsinghua University, the National Scholarship Awarded by the Ministry of Education of the People's Republic of China, and the Outstanding Student Paper Award (1st Place) at the 42nd IEEE International Conference on Plasma Science in 2015. He serves as a frequent reviewer for over 10 journals, including the *Plasma Sources Science and Technology*, the *Physics of Plasmas*, the IEEE TRANSACTIONS ON PLASMA SCIENCE, and the *Journal of Applied Physics*.

Janez Krek (S'14) received the B.Eng. degree in mechanical engineering and the M.Sc. degree in computational plasma physics from the University of Ljubljana, Ljubljana, Slovenia, in 1996 and 2015, respectively. He is currently pursuing the Ph.D. degree with the Department of Computational Mathematics Science and Engineering, Michigan State University, East Lansing, MI, USA.

He is contributing to develop and maintain the OOPD1/PYPD1 (1D3V PIC-MCC), the XOOPIC (2D3V PIC-MCC), and chemical kinetic global model code—the Kinetic Global Model framework. He is currently coupling the KGMf with the Boltzmann equation solver. His current research interests include low-temperature high-pressure plasma simulations and plasma chemical kinetics.

Peng Zhang (S'07–M'12–SM'18) received the B.Eng. and M.Eng. degrees in electrical and electronic engineering from Nanyang Technological University, Singapore, in 2006 and 2008, respectively, and the Ph.D. degree in nuclear engineering and radiological sciences from the University of Michigan (UM), Ann Arbor, MI, USA, in 2012.

He was an Assistant Research Scientist with the Department of Nuclear Engineering and Radiological Sciences, UM. He is currently an Assistant Professor with the Department of Electrical and Computer Engineering, Michigan State University (MSU), East Lansing, MI, USA. He has authored refereed journal publications on electrical contacts, thin films, classical, ballistic, and quantum diodes, space-charge-limited current flows, beam-circuit interaction, multipactor and breakdown, microwave absorption on rough surfaces, slow wave structures, z-pinches, laser-plasma interaction, and more recently on vacuum nanodevices, quantum tunneling plasmonic junctions, ultrafast photoemission, and novel miniaturized electromagnetic radiation sources. His current research interests include theoretical and computational physics in nanoelectronics, plasmas, and accelerator technology.

Dr. Zhang is currently serving as an Editorial Board Member for *Scientific Reports*, a Journal by *Nature* and *Plasma Research Express*, a Journal by the Institute of Physics. He was a recipient of the AFOSR Young Investigator Program Award, the UM Richard and Eleanor Towner Prize for Outstanding Ph.D. Research, the UM Rackham Presidential Fellowship Award, and the IEEE Nuclear and Plasma Sciences Graduate Scholarship Award.

John P. Verboncoeur (M'96–SM'08–F'13) received the B.S. degree in engineering science from the University of Florida, Gainesville, FL, USA, in 1986, and the M.S. and Ph.D. degrees in nuclear engineering from the University of California at Berkeley (UCB), Berkeley, CA, USA.

He was a Post-Doctoral Researcher with the Lawrence Livermore National Laboratory, Livermore, CA, USA, and with the Department of Electrical Engineering and Computer Science (EECS), UCB. He was an Associate Research Engineer with EECS, UCB, where he was a Nuclear Engineering Faculty in 2001 and a Full Professor in 2008. From 2001 to 2010, he served as the Chair for the Computational Engineering Science Program, UCB. In 2011, he joined Michigan State University (MSU), East Lansing, MI, USA, as a Professor of Electrical and Computer Engineering, where he was a Professor of computational mathematics, science, and engineering in 2015. He has authored or co-authored in MSU (formerly Berkeley) suite of particle-in-cell Monte Carlo codes, including XPDP1 and XOOPIC, used by over 1000 researchers worldwide with over 350 journal publications in the last decade, 350 journal articles and conference papers, with over 3500 citations, and has taught 13 international workshops and minicourses on plasma simulation. His current research interests include theoretical and computational plasma physics, with a broad range of applications spanning low-temperature plasmas for lighting, thrusters, and materials processing to hot plasmas for fusion, from ultracold plasmas to particle accelerators, from beams to pulsed power, from intense kinetic nonequilibrium plasmas to high-power microwaves.

Dr. Verboncoeur was a Past-President of the IEEE Nuclear and Plasma Science Society and an IEEE Director-Elect. He was a recipient of the DOE Magnetic Fusion Energy Technology Fellowship. He is currently an Associate Editor of the *Physics of Plasmas*. He has served as a Guest Editor and/or a frequent reviewer for the IEEE TRANSACTIONS ON PLASMA SCIENCE, the IEEE TRANSACTIONS ON ELECTRON DEVICES, as well as a number of other plasma and computational journals.